Nuclear structure study of some bubble nuclei in the light mass region using mean field formalism

Mahesh K. Sharma[1;1)] R. N. Panda[2;2)] Manoj K. Sharma[1;3)] S. K. Patra[3;4)]

[1] School of Physics and Material Sciences, Thapar University, 147 004 Patiala, India
[2] Department of Physics, ITER, Siksha O Anusandhan University, 751 030 Bhubaneswar, India
[3] Institute of Physics, Sachivalaya Marg, 751 005 Bhubaneswar, India

Abstract: We study the structural properties of some light mass nuclei using two different formalisms (i) a recently developed simple effective interaction in the frame work of microscopic non-relativistic Hartree-Fock method and (ii) the well-known relativistic mean field approach with NL3 parameter set. The bulk properties like binding energy, root mean square radii and quadrupole deformation parameter are estimated and compared with the available experimental data. The predicted results of both the formalisms are well comparable with the experimental observations. The analysis of density profiles of these light mass nuclei suggest that ^{22}O, ^{23}F, ^{34}Si and ^{46}Ar have bubble like structure.

Key words: binding energy, charge radius, relativistic mean field, simple effective interaction, non-relativistic mean fields

PACS: 21.10.Dr, 21.10.Ft, 21.60.-n **DOI:** 10.1088/1674-1137/39/6/064102

1 Introduction

The advancement in radioactive ion beams (RIB) at intermediate energy make it possible to explore the nuclear chart. The proton side of the drip line is explored much better compared to the neutron counter part but still most of the region needs to be resurveyed. Numerous exotic phenomenon have been found in these days, and those around the drip-line are of immense interest of us [1–3]. Although the drip-line is well established for doubly magic ^{24}O nuclei (Z=8, N=16) [4], the study of unbound oxygen isotopes [5] suggests the possibility of shifting the drip line. The first observation regards the existence of ^{40}Mg and ^{42}Al isotopes [6] beyond the drip-line given by various mass formulae challenge the earlier predictions and still the investigation of drip-line concept is a challenge for the nuclear science community. One of the interesting phenomena observed these days is the bubble structure of some nuclei like ^{22}O, ^{23}F, ^{34}Si, ^{36}S, ^{36}Ar, ^{46}Ar, ^{84}Se, ^{134}Ce, ^{174}Yb, ^{200}Hg etc. [7–9]. The densities of such cases is depleted from the center. The idea of the bubble effect has been given by Wilson [10]. This phenomenon has greater interest, because it changes the shape of the density distribution from normal nuclei due to different mean field potential. The possibility of formation of bubble nuclei has been studied by various nuclear models. The microscopic calculations using Skyrme Hartree-Fock (SHF) formalism have been carried out to investigate this effect for various regions in Refs. [11–13]. Recently the relativistic and non-relativistic mean field formalism have been used to investigate such effect in the light [14] and superheavy regions [15].

The paper is organized as follows: Section 1 contains a brief introduction and Section 2 containing description of the relativistic and non-relativistic mean field formalisms. The calculations and results are presented in Section 3. The predictability of recently developed HF(SEI-I) model to explore different features of nuclei are included in this section along with the possible candidates of bubble structure of considered nuclei. Finally the summary and conclusions are outlined in Section 4.

2 Formalisms

The structural properties are investigated using the well-known non-relativistic mean field with newly developed simple effective interaction (SEI-I) and relativistic mean field (RMF) formalism. The detailed description of these formalisms are given below:

2.1 Hartree-Fock approximation with simple effective interactions

The simple effective interaction (SEI), like a hybrid

Received 22 September 2014

1) E-mail: maheshphy82@gmail.com
2) E-mail: rnpanda@iopb.res.in
3) E-mail: msharma@thapar.edu
4) E-mail: patra@iopb.res.in

of Gogny and Skyrme, is used to study the bulk properties of finite nuclei within the framework of Hartree-Fock (HF) formalism. The form of SEI is given by [16, 17]

$$\begin{aligned}\nu_{\rm eff}(r) =\ & t_0(1+x_0P_\sigma)\delta(r)\\ &+t_3(1+x_3P_\sigma)\left(\frac{\rho(R)}{1+b\rho(R)}\right)^\gamma\delta(r)\\ &+(W+BP_\sigma-HP_\tau-MP_\sigma P_\tau)f(r), \end{aligned}\quad (1)$$

where $f(r)$ is the functional form of the finite range interaction in terms of Gaussian function $f(r)=\mathrm{e}^{-r^2/\alpha^2}$ which contains a single range parameter α. The other terms have their usual meanings [16]. The Hamiltonian density functional using simple effective interaction is written as

$$\begin{aligned}\mathcal{H} =\ & \mathcal{K}+\mathcal{H}^{\rm Nucl}+\mathcal{H}^{\rm SO}(\boldsymbol{r})\\ &+\mathcal{H}^{\rm Coul}(\mathbf{r})+\mathcal{H}^{\rm RC}. \end{aligned}\quad (2)$$

$\mathcal{K}=\dfrac{\hbar^2}{2m}(\tau_{\rm n}+\tau_{\rm p})$ is the kinetic energy term with $\tau_{\rm n}$ and $\tau_{\rm p}$ are the proton and neutron kinetic energy densities of nucleus. The second term of the Hamiltonian is the nuclear contribution which contains the direct and exchange part. The direct contribution of nuclear energy density comes from the central part of the effective interaction. The third term, the spin-orbit interaction is written as

$$\begin{aligned}\mathcal{H}^{\rm SO}(\boldsymbol{r}) =\ & \frac{-1}{2}W_0[\rho(\boldsymbol{r})\nabla\boldsymbol{J}+\rho_{\rm n}(\boldsymbol{r})\nabla\boldsymbol{J}_{\rm n}\\ &+\rho_{\rm p}(\boldsymbol{r})\nabla\boldsymbol{J}_{\rm p}]. \end{aligned}\quad (3)$$

The fourth term is due to Coulomb interaction containing both direct and exchange terms and is given by

$$\mathcal{H}^{\rm Coul}(\boldsymbol{r}) = \frac{1}{2}\int\frac{\rho_{\rm p}(\acute{\boldsymbol{r}})}{|\boldsymbol{r}-\acute{\boldsymbol{r}}|}\mathrm{d}^3\acute{r}-\frac{3}{4}\left(\frac{3}{\pi}\right)^{1/3}\rho_{\rm p}^{4/3}. \quad (4)$$

The last term of the equation arises from the zero range part of the SEI, which plays the role of residual correlation energy.

$$\begin{aligned}\mathcal{H}^{\rm RC} =\ & \frac{t_0}{4}\int[(1-x_0)[\rho_{\rm n}^2(\boldsymbol{r})+\rho_{\rm p}^2(\boldsymbol{r})]]\\ &+\frac{t_0}{4}\int[(4+2x_0)\rho_{\rm n}(\boldsymbol{r})\rho_{\rm p}(\boldsymbol{r})]\\ &+\frac{t_3}{24}\int[(1-x_3)[\rho_{\rm n}^2(\boldsymbol{r})+\rho_{\rm p}^2(\boldsymbol{r})]]\\ &+\frac{t_3}{24}\int[(4+2x_3)\rho_{\rm n}(\boldsymbol{r})\rho_{\rm p}(\boldsymbol{r})]\left(\frac{\rho(\boldsymbol{r})}{1+b\rho(\boldsymbol{r})}\right)^\gamma. \end{aligned}\quad (5)$$

Here $\rho_{\rm n}$, $\rho_{\rm p}$, ρ, $J_{\rm n}$, $J_{\rm p}$ and J are the neutron, proton and total nuclear and current densities respectively. The 12 parameters γ, b, t_0, t_3, x_0, x_3, W, B, H, M, α and W_0 are used for the calculation of ground state properties. The detailed procedure of calculations for ground state properties like binding energy, charge radius, nuclear matter radius etc. and parameters may be seen in Ref. [16].

2.2 Relativistic mean field Lagrangian density

The relativistic mean field formalism is well documented in Refs. [18–22]. The basic ingredient of RMF model is the relativistic Lagrangian density for a nucleon-meson many body system which is defined as [18–20]

$$\begin{aligned}\mathcal{L} =\ & \overline{\psi}_{\rm i}(\mathrm{i}\gamma^\mu\partial_\mu-M)\psi_{\rm i}+\frac{1}{2}\partial^\mu\sigma\partial_\mu\sigma\\ &-\frac{1}{2}m_\sigma^2\sigma^2-\frac{1}{3}g_2\sigma^3-\frac{1}{4}g_3\sigma^4-g_{\rm s}\overline{\psi}_{\rm i}\psi_{\rm i}\sigma\\ &-\frac{1}{4}\Omega^{\mu\nu}\Omega_{\mu\nu}+\frac{1}{2}m_{\rm w}^2V^\mu V_\mu\\ &-g_\omega\overline{\psi}_{\rm i}\gamma^\mu\psi_{\rm i}V_{\rm \mu}-\frac{1}{4}\boldsymbol{B}^{\mu\nu}.\boldsymbol{B}_{\mu\nu}\\ &+\frac{1}{2}m_\rho^2\boldsymbol{R}^\mu.\boldsymbol{R}_\mu-g_\rho\overline{\psi}_{\rm i}\gamma^\mu\boldsymbol{\tau}\psi_{\rm i}.\boldsymbol{R}^\mu\\ &-\frac{1}{4}F^{\mu\nu}F_{\mu\nu}-e\overline{\psi}_{\rm i}\gamma^\mu\frac{(1-\tau_{3\rm i})}{2}\psi_{\rm i}A_\mu. \end{aligned}\quad (6)$$

Here σ, V_μ and $\boldsymbol{R}_\mu$ are the fields for σ-, ω- and ρ-meson respectively. A^μ is the electromagnetic field. The $\psi_{\rm i}$ are the Dirac spinors for the nucleons whose third component of isospin is denoted by $\tau_{3\rm i}$. $g_{\rm s}$, g_ω, g_ρ and $\dfrac{e^2}{4\pi}=\dfrac{1}{137}$ are the coupling constants for the linear term of σ-, ω- and ρ-mesons and photons respectively. g_2 and g_3 are the parameters for the non-linear terms of the σ-meson. M, m_σ, m_ω and m_ρ are the masses of the nucleons, σ-, ω- and ρ-mesons, respectively. $\Omega^{\mu\nu}$, $\boldsymbol{B}^{\mu\nu}$ and $F^{\mu\nu}$ are the field tensors for the V^μ, $\boldsymbol{R}^\mu$ and the photon fields, respectively. Now we used two assumptions, first the nucleons are moving inside the nucleus in a spherically symmetric potential. In this case, the large and small components of Dirac spinor $\psi_{\rm i}$ are expanded separately in terms of radial function of a spherical harmonic oscillator potential and in a second assumption, the nucleons are moving in non-spherical symmetric potential. In this case the large and small components of the Dirac spinor are expanded in axial symmetric manner in term of deformed harmonic oscillator potential by taking volume conservation into account. The set of Dirac and Klein-Gordon equations are solved by these two assumptions to obtain the bulk properties of nuclei. The quadrupole moment deformation parameter (β_2), root mean square radii ($r_{\rm m}$) and binding energy (B.E.) are evaluated using the standard relations [20].

2.3 Pairing correlation

The constant gap, BCS-approach is reasonably valid for nuclei in the valley of β-stability line for determining the bulk properties like B.E., nuclear radii and quadrupole deformation parameter [23]. The pairing energy can be given as:

$$E_{\rm pair}=-G\left[\sum_{i>0}u_iv_i\right]^2. \quad (7)$$

where G is a pairing force constant, v_i^2 and $u_i^2=1-v_i^2$ are the occupation probabilities [24, 25]. The variational approach with respect to v_i^2 gives the BCS equation [24].

$$2\epsilon_i u_i v_1-\Delta(u_i^2-v_i^2)=0, \tag{8}$$

using $\Delta=G\sum_{i>0}u_i v_i$. The occupation number is defined as:

$$n_i=v_i^2=\frac{1}{2}\left[1-\frac{\epsilon_i-\lambda}{\sqrt{(\epsilon_i-\lambda)^2+\Delta^2}}\right]. \tag{9}$$

The chemical potentials $\lambda_{\rm n}$ and $\lambda_{\rm p}$ are determined by the particle numbers for neutrons and protons. The pairing energy is computed as

$$E_{\rm pair}=-\Delta\sum_{i>0}u_i v_i.$$

For a particular value of Δ and G, the pairing energy $E_{\rm pair}$ diverges, if it is extended to an infinite configuration space. In fact, for all realistic calculations with finite range forces, Δ decreases with states for large momenta near the Fermi surface. We used pairing window, where the equations are extended upto the level $|\epsilon_i-\lambda|\leqslant 2(41A^{\frac{-1}{3}})$. The factor of 2 has been determined so as to reproduce the pairing correlation for neutrons in ^{118}Sn using Gogny force [25–27]. The values of $\Delta_{\rm n}$ and $\Delta_{\rm p}$ are taken as inputs of the BCS-equation [28]. These constant gaps for neutrons and protons are given as:

$$\Delta_{\rm p}({\rm MeV}) = RB_{\rm s}{\rm e}^{sI-tI^2}/Z^{1/3}, \tag{10}$$

$$\Delta_{\rm n}({\rm MeV}) = RB_{\rm s}{\rm e}^{-sI-tI^2}/A^{1/3}, \tag{11}$$

with R=5.72 MeV, s=0.118, t=8.12, $B_{\rm s}$=1 and $I=(N-Z)/(N+Z)$. The exponential terms take into the account the dependencies of neutron-proton excess and shape of the nucleus.

3 Results and discussions

3.1 Ground state properties

The bulk properties are very important for the characteristics study of nuclear systems. We have used RMF(NL3) [19–21, 29] and HF(SEI-I) [16, 17] formalism to explain the nuclear bulk properties like B.E., rms charge radii ($r_{\rm c}$) and quadrupole deformation parameter (β_2) for the considered nuclei. We follow the numerical procedure of Refs. [30, 31] for spherical RMF(NL3) and Refs. [20, 22, 26, 32] for deformed cases. The evaluation procedure of SEI is given in Ref. [16, 17].

3.1.1 Binding energy

The binding energies (B.E.s) of $^{9-12}$Be, $^{12-15}$B, $^{12-20}$C, $^{20-23}$N, $^{20-24}$O, $^{23-27}$F, $^{28-32}$Ne, $^{32-35}$Mg, $^{32-35}$Si, $^{34-37}$S and $^{34-48}$Ar obtained by relativistic mean field theory using spherical and axially deformed coordinates systems and with non-relativistic mean field theory using simple effective interaction are presented in Table 1 along with experimental values [33, 34]. The B.E. of ^{10}Be are 65.302, 63.49 and 64.855 MeV for HF(SEI-I), Sph. RMF(NL3) and Def. RMF(NL3) solutions, well comparable to its experimental value 64.970 MeV. Hence by examining the results of this table, one may conclude that both the formalisms are capable of reproducing the experimental data of binding energy for the considered nuclei.

3.1.2 Charge radius

The calculated root mean square charge radius ($r_{\rm c}$) of $^{9-12}$Be, $^{12-15}$B, $^{12-20}$C, $^{20-23}$N, $^{20-24}$O, $^{23-27}$F, $^{28-32}$Ne, $^{32-35}$Mg, $^{32-35}$Si, $^{34-37}$S and $^{34-48}$Ar nuclei from both RMF(NL3) and non-relativistic HF(SEI-I) mean field theories are presented in Table 1. The experimental data are also given for comparison wherever available [35]. The rms proton radius $r_{\rm p}$ is obtained using the distribution of point protons inside the nucleus. The charge radius $r_{\rm c}$ is calculated by taking the finite size 0.8 fm of the proton, which is evaluated from the formula $r_{\rm c}=\sqrt{r_{\rm p}^2+0.06}$ [20]. The calculated values of $r_{\rm c}$ for ^{11}Be are 2.329, 2.479 and 2.449 fm from HF(SEI-I), Sph. RMF(NL3) and Def. RMF(NL3) formalism, which are well comparable with the experimental value of 2.46 fm. Similarly, $r_{\rm c}$ for ^{36}Ar and ^{46}Ar are 3.035, 3.373 for HF(SEI-I), 3.388, 3.410 for Sph. RMF(Nl3), 3.379, 3.415 for Def. RMF(NL3) and 3.390, 3.437 in Fermi scale for experimental observations, respectively. In general, observation of this table signifies the predictability of these theories as they show comparable results with experimental data.

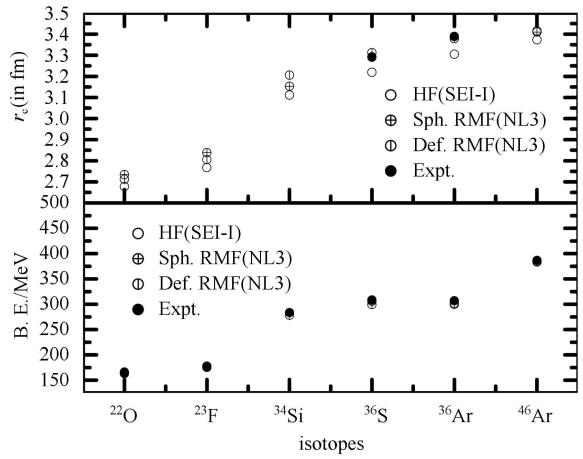

Fig. 1. B.E. and charge radius of ^{22}O, ^{23}F, ^{34}Si, ^{36}S, ^{36}Ar and ^{46}Ar bubble nuclei with experimental data [33–35].

3.1.3 Quadrupole deformation parameter β_2

Table 1 also present the values of deformation along with the experimental data [36] wherever available. The

Table 1. The ground state properties of light mass nuclei obtained from RMF(NL3) and HF(SEI-I) calculations are compared with experimental data wherever available. The binding energy (B.E.) is in MeV and charge radius r_c is in fm.

nuclei	B.E.				r_c				β_2	
	HF(SEI-I) (Sph.)	RMF(NL3) (Sph.)	RMF(NL3) (Def.)	Expt.[33, 34]	HF(SEI) (Sph.)	RMF(NL3) (Sph.)	RMF(NL3) (Def.)	Expt.[35]	RMF(NL3) (Def.)	Expt.[36]
^{9}Be	54.927	54.76	58.018	58.164±0.000	2.305	2.461	2.510	2.519	0.793	
^{10}Be	65.302	63.49	64.855	64.970±0.000	2.302	2.537	2.423	2.36	0.509	
^{11}Be	69.380	67.97	67.780	65.478±0.000	2.329	2.479	2.449	2.46	0.369	
^{12}Be	73.190	73.61	71.378	68.649±0.004	2.353	2.549	2.450		−0.137	
^{12}B	82.172	82.85	82.176	79.575±0.001	2.393	2.498	2.457		0.168	
^{13}B	88.250	88.84	88.842	84.453±0.001	2.411	2.540	2.492		0.097	
^{14}B	89.256	91.88	89.874	85.423±0.021	2.423	2.534	2.522		0.382	
^{15}B	90.162	93.64	92.593	88.194±0.022	2.435	2.532	2.564	2.511	0.611	
^{12}C	88.422	88.23	91.349	92.160±1.700	2.436	2.364	2.310	2.47	0.007	0.577(16)
^{13}C	97.489	96.31	98.098	97.108±0.000	2.454	2.459	2.466	2.46	−0.000	
^{14}C	105.829	104.38	106.929	105.284±0.000	2.470	2.504	2.517	2.56	0.000	0.36(3)
^{15}C	108.846	108.66	108.477	106.502±0.000	2.480	2.516	2.535		0.249	
^{16}C	111.642	113.45	111.874	110.752±0.003	2.489	2.531	2.565		0.448	
^{17}C	114.248	116.40	114.083	111.486±0.017	2.500	2.542	2.582		0.458	
^{18}C	116.709	118.79	116.842	115.670±0.030	2.509	2.552	2.601		0.471	
^{19}C	119.015	119.91	119.511	116.242±0.100	2.521	2.562	2.629		−0.438	
^{20}C	121.154	122.54	119.736	119.18±0.200	2.532	2.573	2.590		0.278	
^{20}N	139.487	139.37	136.772	134.184±0.055	2.605	2.671	2.683		−0.306	
^{21}N	143.095	142.59	141.475	138.768±0.100	2.614	2.674	2.694		−0.311	
^{22}N	146.205	145.55	143.948	140.052±0.200	2.624	2.679	2.678		−0.159	
^{23}N	148.765	148.17	147.864	141.726±0.300	2.637	2.687	2.674		−0.009	
^{20}O	154.043	152.71	151.585	151.36±0.100	2.668	2.720	2.726		0.250	0.268(6)
^{21}O	159.645	157.95	156.944	158.928±0.100	2.673	2.721	2.716		0.132	
^{22}O	164.758	164.18	163.192	166.496±0.100	2.678	2.735	2.712		0.002	0.19(4)
^{23}O	169.040	168.32	167.227	174.064±0.100	2.689	2.741	2.725		0.003	
^{24}O	172.508	171.87	171.665	181.632±0.100	2.701	2.752	2.737		0.003	
^{23}F	177.956	176.75	175.378	175.283±0.100	2.768	2.839	2.805		−0.188	
^{24}F	183.433	182.06	180.162	179.11±0.100	2.778	2.838	2.812		−0.128	
^{25}F	186.026	186.90	185.221	183.375±0.100	2.782	2.853	2.821		−0.087	
^{26}F	188.890	191.76	187.928	184.158±0.100	2.806	2.875	2.852		−0.125	
^{27}F	191.507	195.00	191.245	186.246±0.200	2.827	2.891	2.886		0.151	
^{28}Ne	207.273	210.62	208.122	206.89± 0.100	2.892	2.964	2.966	2.963	0.223	0.36(3)
^{29}Ne	210.833	214.35	211.140	207.843±0.100	2.912	2.982	2.981		0.159	
^{30}Ne	214.160	218.02	214.920	211.29±0.300	2.933	2.998	2.999		0.098	0.49(17)
^{31}Ne	214.569	221.97	215.812	211.42±0.200	2.944	3.012	3.032		0.238	
^{32}Ne	214.860	223.95	218.409	213.472±0.500	2.956	3.024	3.071		0.363	
^{32}Mg	249.390	252.06	250.387	249.804±0.200	3.032	3.095	3.091	3.186	0.119	0.51(5)
^{33}Mg	252.015	256.02	252.982	252.017±0.200	3.043	3.107	3.118		0.231	
^{34}Mg	254.355	259.14	257.169	256.462±0.100	3.053	3.118	3.151		0.340	0.55(6)
^{35}Mg	256.498	261.82	260.211	257.460±0.200	3.064	3.129	3.174		0.385	
^{32}Si	267.928	267.69	268.203	271.407±0.000	3.078	3.113	3.141		−0.203	0.26(4)
^{33}Si	275.953	275.97	275.359	275.915±0.000	3.095	3.133	3.134		−0.085	
^{34}Si	283.470	283.78	278.249	283.428±0.014	3.111	3.153	3.206		−0.337	0.18(4)
^{35}Si	288.258	289.77	287.135	285.903±0.038	3.119	3.163	3.164		−0.084	
^{34}S	286.424	286.05	286.295	291.838±0.000	3.199	3.270	3.259	3.28	−0.168	0.247(3)
^{35}S	296.491	296.71	295.543	298.824±0.000	3.209	3.282	3.262		−0.077	
^{36}S	305.978	306.52	299.502	308.714±0.000	3.219	3.293	3.312	3.29	−0.309	0.157(7)
^{37}S	312.676	313.58	309.946	313.017±0.000	3.224	3.299	3.290		−0.116	
^{34}Ar	273.357	273.76	273.397	278.719±0.000	3.295	3.387	3.360	3.365	−0.168	0.229(15)
^{36}Ar	300.129	300.25	302.268	306.716±0.000	3.305	3.388	3.379	3.390	−0.209	0.253(8)
^{38}Ar	324.432	325.59	319.946	327.342±0.000	3.318	3.397	3.396	3.402	−0.279	0.161(4)
^{40}Ar	341.555	342.31	340.945	343.810±0.000	3.326	3.401	3.392	3.427	−0.160	0.269(5)
^{42}Ar	357.013	357.39	356.393	359.335±0.005	3.335	3.406	3.402	3.435	−0.176	0.27(3)
^{44}Ar	371.135	371.42	370.639	373.728±0.001	3.345	3.410	3.410	3.445	−0.179	0.22(16)
^{46}Ar	383.672	384.57	384.603	386.927±0.040	3.373	3.410	3.415	3.437	−0.167	0.170(17)
^{48}Ar	391.79	394.58	392.810	396±0.720	3.393	3.437	3.442		−0.198	

negative β_2 values of nuclei in this table signify oblate deformation, whereas positive values predict the prolate deformation and zero represent the spherical behavior. It is worth mentioning that the NL3 parameter set does not give a converged solution for some of the light mass nuclei such as ^{12}C and ^{14}C. To get a converged result for such cases, we use the BCS pairing approach with a small but finite value of the pairing strength $\Delta_{\rm n,p}$. As a result, the value of B.E. for ^{12}C is 91.349 and for ^{14}C is 106.929, which are both in nice agreement with experimental data of 92.160±1.7 and 105.285±0.00, respectively. But the values of quadrupole deformations are 0.007, 0.000, which have a large deviation with respect to experimental values 0.577(16), 0.36(3). So we compromise a bit in the quadrupole deformation for such cases. In a recent paper [37] we have observed that, for both NL3 and SkI4 force parameter sets in the light mass region, pairing is less important for the majority of cases. It is also observed that the deformation becomes negligible for ^{20}Ne and do not agree with experimental deformation parameter if one includes pairing. On the other hand, without pairing, the deformation parameter is reproduced substantially well as density of states near the Fermi surface are small and do not require pairing for such light mass nuclei as it is considered here. The authors of paper [37] concluded that the deformation parameters start affecting experimental data if one ignores pairing in this mass region. In the present work we have performed the calculations for most of the nuclear systems without considering pairing effects due to this reason.

3.2 Bubble nuclei

The bubble effect has appeared in some of the nuclei, where the density of nucleus is depleted at the central part. The main mechanism for the formation of bubble nuclei is the lack of particles at the centre of nucleus which causes the s levels to be less bound than observed in the usual cases with the uniform density distribution.

Figure 1 represents the B. E. and charge radius ($r_{\rm c}$) of ^{22}O, ^{23}F, ^{34}Si, ^{36}S, ^{36}Ar and ^{46}Ar bubble nuclei obtained from HF(SEI-I), sph RMF(NL3) and def RMF(NL3) formalism along with the experimental data. The values of B.E. and charge radius are also given in Table 1. The upper panel of the figure shows the charge radius and lower panel B. E. of selected cases with the experimental data wherever it is available. This figure suggests that both the formalism relativistic mean field and the non-relativistic mean field are capable of reproducing the bulk properties of such cases.

Close inspection of the figure suggests the results obtained with relativistic mean field formalism are close to the experimental values in comparison to the non-relativistic mean field formalism.

3.2.1 Density

Figure 2 represents the densities of the considered set of bubble nuclei as a function of radial distance (r in fm). In normal cases, nucleon distribution inside the nucleus is maximum at the center and starts decreasing continuously towards the surface. Keen inspection of Fig. 2 indicates that the considered set of nuclei shows depletion of the densities at the centre, which is the primary indication for their bubble structure. It also appears from the figure that densities of the considered set of nuclei shows a similar kind of trend for all the formalisms.

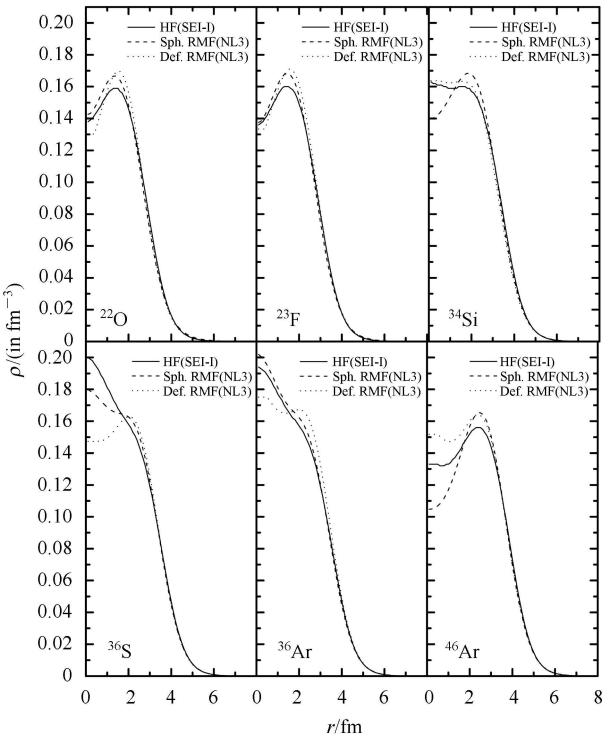

Fig. 2. Radial density plots of ^{22}O, ^{23}F, ^{34}Si, ^{36}S, ^{36}Ar and ^{46}Ar bubble nuclei using HF(SEI-I), Sph RMF(NL3) and def RMF(NL3) formalism.

Figure 3 shows the proton and neutron density distributions of ^{22}O, ^{23}F, ^{34}Si, ^{36}S, ^{36}Ar and ^{46}Ar as a function of radial distance. The left panel of the figure shows the neutron and the right panel shows the proton density distribution of these bubble cases for HF(SEI-I), Sph. RMF(NL3) and Def. RMF(NL3) densities, respectively. It is clear from the figure that the depletion for proton density distribution is more than the neutron counterpart. This may be due to the Coulomb repulsion between protons. So the particles rise high enough in energy and highest s levels will be empty, resulting in depletion of central density of particles as a consequence of which the radius of the nucleus increases.

Table 2. The depletion factor ($D.F.$ in %) of neutron (N), proton (P) and total (T) densities for some probable cases of bubble nuclei obtained from HF(SEI-I), Sph. RMF(NL3) and Def. RMF(NL3).

nuclei	$D.F.$% HF(SEI-I)			$D.F.$% Sph. RMF(NL3)			$D.F.$% Def. RMF(NL3)		
	N	P	T	N	P	T	N	P	T
^{22}O	8.21	19.14	13.21	9.49	20.23	14.46	24.35	22.47	23.29
^{23}F	10.67	20.45	15	14.44	22.71	18.26	22.14	22.30	21.99
^{34}Si	—	36.66	—	0.36	36.27	16.75	—	3.73	—
^{36}S	—	—	—	—	—	—	3.49	16.25	9.49
^{36}Ar	—	—	—	—	—	—	—	—	—
^{46}Ar	—	51.05	14.74	15.31	62.08	36.64	1.56	14.73	7.51

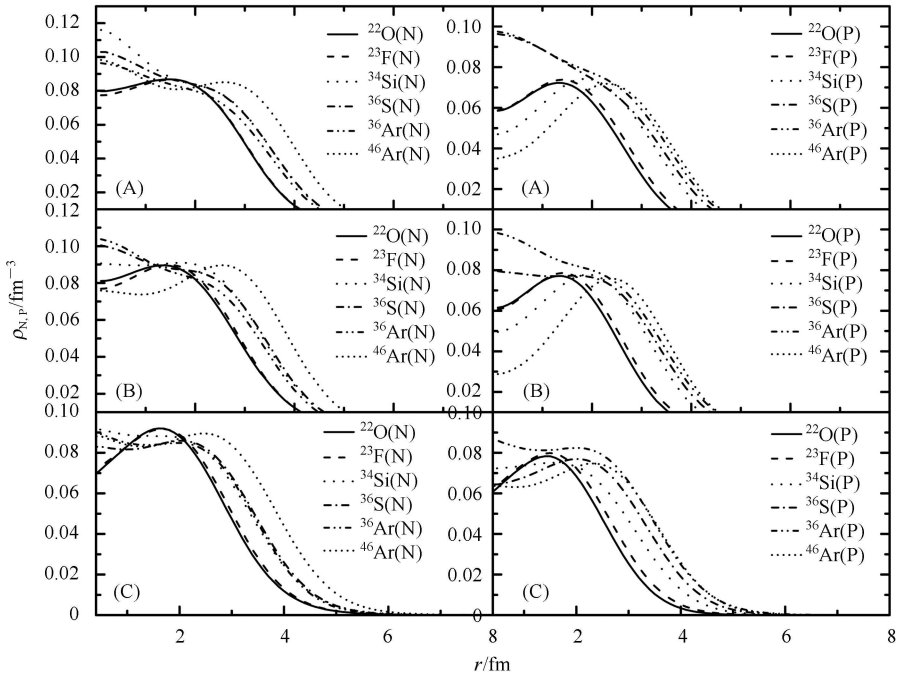

Fig. 3. Radial density plots for expected bubble nuclei ^{22}O, ^{23}F, ^{34}Si, ^{36}S, ^{36}Ar and ^{46}Ar obtained by (A) HF(SEI-I) (B) Sph. RMF(NL3) (C) Def. RMF(NL3) formalism.

The depleted density of nuclei has been measured in term of depletion factor ($D.\ F.$) defined as [7]

$$D.F.=\frac{\rho_{\max}-\rho_{\rm cen}}{\rho_{\max}}, \tag{12}$$

where $\rho_{\max}$ and $\rho_{\rm cen}$ represent the values of maximum and the central density. The calculated values of $D.\ F.$ in % for the ^{22}O, ^{23}F, ^{34}Si, ^{36}S, ^{36}Ar and ^{46}Ar are presented in Table 3. The value of $(D.F.)_{\rm T}$ in % for ^{22}O are 13.21, 14.46 and 23.28 for the HF(SEI-I), Sph. RMF(NL3) and Def. RMF(NL3) densities. Similarly the $(D.F.)_{\rm T}$ for the ^{23}F are 15, 18.26 and 21.99 from same densities, respectively. The $(D.F.)_{\rm P}$ in % for the ^{34}Si and ^{46}Ar nuclei are 36.36 and 51.06 for HF(SEI-I), 36.27 and 62.08 for Sph. RMF(NL3) and 3.72 and 14.72 for Def. RMF(NL3) densities which clearly indicate the nature of their proton bubble. This table also signifies that no bubble effect is seen for ^{36}Ar, whereas 16.25% $(D.F.)_{\rm P}$ for ^{36}S in Def. RMF(NL3) indicate that it may be a case for proton bubble along with ^{34}Si and ^{46}Ar nuclei. Thus prominent cases having bubble effects are observed to be ^{22}O, ^{23}F, ^{34}Si and ^{46}Ar.

4 Summary and conclusions

In summary, we have studied the structural properties of $^{9-12}$Be, $^{12-15}$B, $^{13-20}$C, $^{20-23}$N, $^{20-24}$O, $^{23-27}$F, $^{28-32}$Ne, $^{32-35}$Mg, $^{32-35}$Si, $^{34-37}$S and $^{34-48}$Ar in the frame work of non-relativistic Hartree-Fock with simple effective interaction and relativistic mean field formalism in the light mass region. The bulk properties such as binding energy, charge radius and quadrupole de-

formation parameter β_2 show good agreement with the experimental data. The bubble effect for ^{22}O, ^{23}F, ^{34}Si, ^{36}S, ^{36}Ar and ^{46}Ar nuclei in light mass region is studied. The prominent cases having bubble effects are observed to be ^{22}O, ^{23}F, ^{34}Si and ^{46}Ar from our study. This will affect studies of nuclear structure in the drip-line and superheavy regions. In general, we observed that both the formalisms are capable of studying the nuclear structure for most of the light mass nuclei, with slightly better accuracy for RMF formalism over the non-relativistic HF(SEI-I). Further investigations in the medium and heavy mass regions may impart better description regarding the comparative analysis of these formalisms.

One of the authors, MKS, thanks the Institute of Physics, Bhubaneswar, for kind hospitality.

References

1 Patra S K, Praharaj C R. arXiv: [Nucl. th], 2010, **v1**: 1002.0654
2 Saxena G, Singh D. Int. J. Mod. Phys. E, 2013, **22**: 1350025
3 Singh S K, Mahapatra S, Mishra R N. Int. J. Mod. Phys. E, 2013, **22**: 1350018
4 Ozawa A et al. Phys. Rev. Lett., 2000, **84**: 5493
5 Caesar C et al. Phys. Rev. C, 2013, **88**: 034313
6 Baumann T et al. Nature, 2007, **449**: 1022
7 Grasso M et al. Int. J. Mod. Phys. E, 2009, **18**: 2099
8 Grasso M et al. Phys. Rev. C, 2009, **79**: 034318
9 Davies K T R, Wong C Y, Krieger S J. Phys. Lett. B, 1972, **41**: 455
10 Wilson H A. Phys. Rev., 1946, **69**: 538
11 Campi X, Sprung D W L. Phys. Lett. B, 1973, **46**: 291
12 Bender M, Rutz K, Reinhard P G, Maruhn J A, Greiner W. Phys. Rev. C, 2003, **60**: 55
13 Decharge J, Berger J F, Girod M, Dietrich K. Nucl. Phys. A, 2003, **716**: 55
14 Shukla A, Sven A^{0}berg, Patra S K. J. Phys. G: Nucl. Part. Phys., 2011, **38**: 095103
15 Singh S K, Ikram M, Patra S K. Int. J. Mod. Phys. E, 2013, **22**: 135001
16 Behera B, Viñas X, Bhuyan M, Routray T R, Sharma B K, Patra S K. J. Phys. G: Nucl. Part. Phys., 2013, **40**: 095105
17 Routray T R, Viñas X, Tripathy S K, bhuyan M, Patra S K, Behera B. J. Phys. Conf. Ser., 2013, **420**: 012114
18 Boguta J, Bodmer A R. Nucl. Phys. A, 1977, **292**: 413
19 Pannert W, Ring P, Boguta J. Phys. Rev. Lett., 1987, **59**: 2420
20 Patra S K, Praharaj C R. Phys. Rev. C, 1991, **44**: 2552
21 Del Estal M, Centelles M, Vinas X, Patra S K. Phys. Rev. C, 2001, **63**: 024314
22 Ring P. Prog. Part. Nucl. Phys., 1996, **37**: 193
23 Panda R N, Sharma Mahesh K, Patra S K. Mod. Phys. Lett. A, 2014, **29**: 1450013
24 Preston M A, Bhaduri R K. Strutureof Nucleus. Addison-Wesley Publishing Company, Mass Sachusetts, USA, 1975, **8**: 309
25 Patra S K. Phys. Rev. C, 1993, **48**: 1449
26 Serot B D, Walecka J D. Adv. Nucl. Phys., 1986, **16**: 1
27 Decharg J, Gogny D. Phys. Rev. C, 1980, **21**: 1568
28 Madland D G, Nix J R. Nucl. Phys. A, 1981, **476**: 1
29 Lalazissis G A, König J, Ring P. Phys. Rev. C, 1997, **55**: 540
30 Del Estal M, Centelles M, Viñas X, Patra S K. Phys. Rev. C, 2001, **63**: 044321
31 Patra S K, Del Estal M, Centelles M. X.Viñas, Phys. Rev. C, 2001, **63**: 024311
32 Gambhir Y K, Ring P, Thimet A. Ann. Phys. (N.Y), 1990, **198**: 132
33 Audi G, Wapstra A H, Thibault C. Nucl. Phys. A, 2003, **729**: 337
34 http://amdc.in2p3.fr/masstable/Ame 2011int/mass.
35 Angeli I, Marinova K P. Atomic Data and Nuclear Data Table, 2013, **99**: 69
36 National Nuclear Data Center, Brookhven National Laboratory, Based on ENSDF and the Nuclear Wallet Cards
37 Singh S K, Praharaj C R, Patra S K. Cent. Eur. J. Phys., 2014 **12**: 42–56